Pergamon

Journal of Structural Geology, Vol. 17, No. 1, pp. 47 to 58, 1995

0191-8141/95 $9.50+0.00

0191-8141(94)E0027-V

Neogene ongoing tectonics in the Southern Ecuadorian Andes: analysis of the evolution of the stress field

A. LAVENU

ORSTOM, UR 1H-TOA, 213 rue La Fayette, 75480 Paris Cedex 10, France, and Laboratoire de Géodynamique et Modélisation des Bassins, UPPA, 64000 Pau, France

C. NOBLET

BHP Minerals, 550 California Street, San Francisco, CA 94104-1020, U.S.A.

and

TH. WINTER

Coyne et Bellier, 9 allée des Barbanniers, 92632 Gennevilliers Cedex, France

(*Received* 2 *April* 1993; *accepted in revised form* 14 *February* 1994)

Abstract—Microtectonic analysis of infilling deposits in South Ecuadorian Neogene basins brings to light a compressive stress field with $\sigma 1$ along a NNE–SSW to NE–SW direction in the early Miocene, changing to an E–W direction in the Middle and Late Miocene. The syn-sedimentary deformations which affect the deposits of the basins suggest similar stress regimes due to a compressive ongoing tectonic system in the Miocene, for at least 15 Ma. There is a good correlation between rapid convergence in the Neogene and the time period during which the continental South Ecuadorian basins were deformed by compression (Quechua period).

INTRODUCTION

Predominantly continental sedimentation had developed during the Neogene in the Northern Andes (Case 1974, Case *et al.* 1990). This is applicable, particularly in the Ecuadorian Andes, to the basins of Cuenca, Girón, Nabón, Loja, Malacatos and Zumba, formed along major crustal faults in the south of Ecuador (Fig. 1). The Eastern Cordillera is essentially composed of Paleozoic rocks. The Western Cordillera is represented by a series of Mesozoic and Lower Paleogene rocks. Until now, these have been interpreted as belonging to a volcanic arc built on continental crust (Lebrat 1985, Lebrat *et al.* 1985a,b). In the southern part of Western Cordillera, Paleozoic rocks appear in the Amotape Block. During Late Paleogene, both Cordilleras were covered by volcaniclastic deposits. Continental detrital deposits and interstratified volcanic material which comprise the fill of the Neogene basins, overlie a Cretaceous – Upper Oligocene basement. The basins are limited by two families of N–S and N20°–N40° trending faults (all azimuths are from North in clockwise sense, i.e. eastwards). Based on sedimentological analyses and the study of the syn-sedimentary deformation, Noblet *et al.* (1988) have suggested a system of ongoing compressive deformation during the Neogene. The present study is based on a microtectonic analysis of the basins. Its purpose is to characterize the successive stress fields contemporaneous with the basin infilling, to verify their compatibility with the syn-sedimentary deformation,

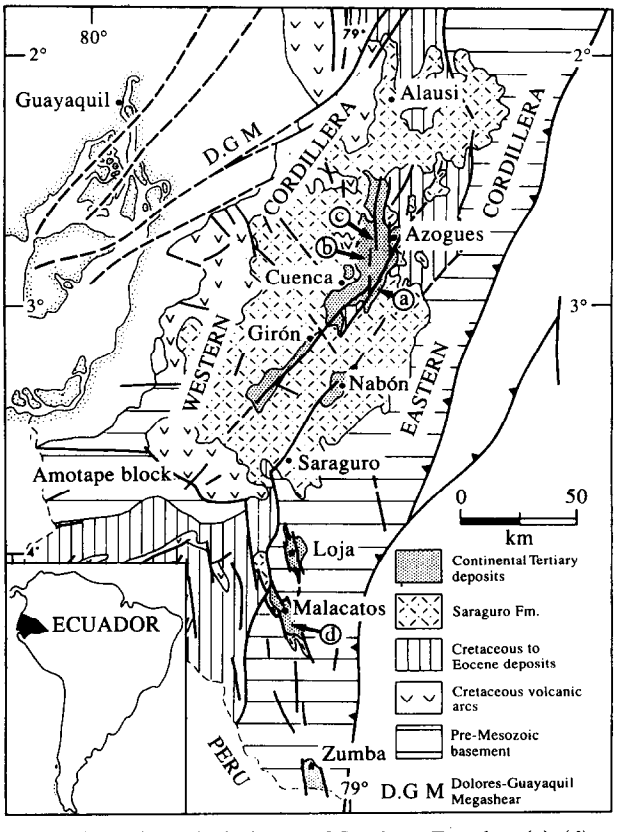

Fig. 1. Schematic geological map of Southern Ecuador. (a)–(d) are related to Fig. 3. Dashed lines are inferred faults. Barbed lines represent the main thrusts in the Subandean zone.

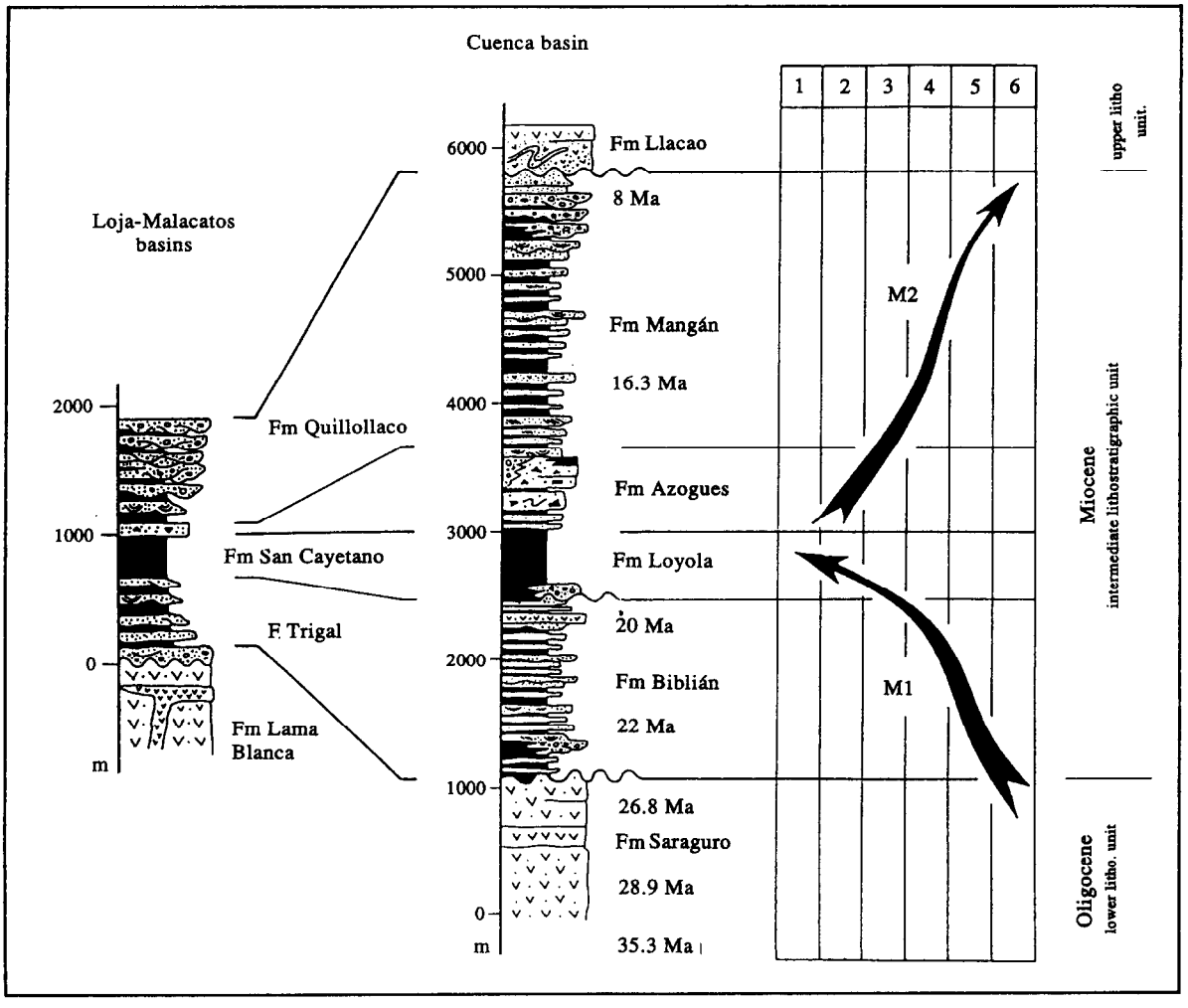

Fig. 2. Synthetic sedimentary evolution of Loja, Malacatos and Cuenca basins. The infilling shows a cyclic sedimentary evolution. The fining and thinning upward in the lower sequence characterizes the basin opening; the coarsening and thickening upward in the upper sequence characterizes its closing. Radiometric ages are from Kennerley (1980), Barberi *et al.* (1988) and Lavenu *et al.* (1992). Depositional environment: (1) distal lacustrine; (2) lacustrine turbidites; (3) lacustrine delta; (4) flood plain; (5) braided rivers; (6) alluvial fan.

and to test the reliability of microtectonic analysis in a context of ongoing tectonics. The results obtained are compared with tectonic events encountered elsewhere in the Northern and Central Andes (Butler 1974, Jordan 1983, Mégard 1987, Burke 1988, Sébrier *et al.* 1988, Daly 1989, Sébrier & Soler 1991).

STRATIGRAPHY AND SEDIMENTOLOGICAL CHARACTERISTICS OF THE BASINS

In the Cuenca basin, the Tertiary rocks can be grouped regionally into three superposed lithostratigraphic units (Bristow 1973, Noblet *et al.* 1988) (Fig. 2). South of the Cuenca Basin, the stratigraphy of the other South Ecuadorian basins was defined by lithological correlation with the stratigraphic column of Cuenca.

The lower lithostratigraphic unit (Saraguro Formation), essentially volcanic, represents the upper part of the basement of the basins. It consists of intermediate and acidic lavas and pyroclastic deposits. Its thickness exceeds 1000 m. Radiometric dating attributes it to the Oligocene: 26.8 ± 0.7 Ma (Kennerley 1980), 28.9 ± 1.4 Ma (Barberi *et al.* 1988), 35.3 ± 0.9 Ma (Lavenu *et al.* 1992) and 29–23 Ma (Winkler *et al.* 1993).

The intermediate lithostratigraphic unit lies unconformably on the basement (Noblet *et al.* 1988, Egüez & Noblet 1988) and corresponds to the Neogene fill of the South Ecuadorian basins. It is composed of alternating conglomerates, sandstones and shales. This unit reaches a thickness of up to 4500 m in the Cuenca Basin, but never exceeds 1500–2000 m in the others. The base of the unit is of Early Miocene age (Bristow 1973, Bristow & Parodiz 1982, Madden 1990). The upper part of the unit has been ascribed to Middle to Late Miocene by paleontological analyses (Marshall & Bowles 1932, Bristow 1973). A sedimentological analysis of South-Ecuadorian basin deposits (intermediate lithological unit) was performed by Noblet *et al.* (1988), Robalino (1988), Lavenu & Noblet (1989), Fierro (1991), Izquierdo (1991) and Mediavilla (1991). This reveals a cycle of sedimentation composed of two sequences, M_1 and M_2, in all the basins. The first sequence, M_1, consists of proximal (alluvial) to distal (lacustrine) deposits. This

sequence is 1500 m-thick in the Cuenca Basin and about 600 m in the southern basins. It decreases, both fining upward and thinning upward. This sequence is characteristic of basin deepening related to large tectonic subsidence (Blair & Bilodeau 1988). The second sequence (M_2) shows a reverse sequence, with coarsening upward and thickening upward from distal (lacustrine) to proximal (alluvial fans) deposits. This second sequence is approximately 3000 m-thick in the Cuenca Basin and 1000 m-thick in the other basins. The sequence represents the tectonic closing of the basins. The sedimentation of this intermediate unit is contemporaneous with an important syn-sedimentary volcanic activity at the basin boundaries as well as within the basins. The rocks observed are mainly andesites, dacites and rhyolites. Lava flows in the Cuenca Basin, known as the 'Descanso Andesite', dated at 19.7 ± 5 Ma and 21 ± 0.6 Ma (Kennerley 1980), and also a monogenetic andesitic breccia, interstratified in the sediments, comprising the top of sequence M_1, dated at 22 ± 0.8 Ma and 24.7 ± 0.6 Ma (Lavenu *et al.* 1992) give evidence of Lower Miocene volcanic activity. In the Nabón Basin, radiometric dates confirm this age: 22 ± 1.3 Ma (Winkler *et al.* 1993). In sequence M_2, radiometric dating on rhyolitic tuffs within the Cuenca Basin (16.3 ± 0.7 Ma; Lavenu *et al.* 1992) indicates acidic volcanic activity during the Middle Miocene. It confirms the radiometric ages obtained outside of the basin (15.4 ± 0.7 to 11.2 ± 0.3 Ma; Barberi *et al.* 1988). A late Miocene–Pliocene volcanic event was also recorded and Barberi *et al.* (1988) attributed an age of 8.0 ± 0.08 Ma to an intercalated dacitic flow near the top of the basin deposits. Clastic deposits of this intermediate lithostratigraphic unit were thus deposited throughout the entire Miocene period.

The upper lithostratigraphic unit (Llacao Formation) unconformably overlies the prior units. This volcaniclastic unit is thin (several tens of meters only), and composed of conglomerates, breccias, and volcanic tuffs. It has been ascribed to the Pleistocene (Bristow 1973, DGGM 1974, Baldock 1982).

SYN-SEDIMENTARY DEFORMATION

Analysis of folding which affected the Cuenca Basin deposits was carried out by Noblet *et al.* (1988) and Lavenu & Noblet (1989). The main results of these studies are discussed below.

During Early Miocene, the sequence M_1 (>1200 m) displays sedimentary wedges which confirm the presence of a tensional component along the N20°–N40° faults during sedimentation (Fig. 3a). M_1 stratification poles indicate an additional deformation, highly localized near the basin boundary. This deformation corresponds to a conical syn-sedimentary fold with a N120°, subvertical hinge line (Fig. 3a). Analysis of stratification poles on only one fold has little statistical significance, especially in a zone where the layers were progressively tilted during sedimentation. Nevertheless, this may be indicative of a near NNE–SSW shortening direction along strike-slip faults, compatible with an extension perpendicular to the N20°–N40° fault during a transpressive tectonic regime (Moody & Hill 1956, Zolnai 1989). Consequently, the basin's opening is characterized by extensive deformation, particularly marked by a tensional (and perhaps tensional strike-slip) component along N20°–N40° faults throughout the deposition of sequence M_1.

During Early to Middle Miocene, conical syn-sedimentary folds occurred in the basal 300–400 m deposits comprising sequence M_2 (Fig. 3b). The fold hinge lines, deduced from statistical analyses of stratification poles, have been untilted by the dip and direction of the first folded beds. The untilted hinge lines plunge about 15°–N150° implying a shortening direction of N60°. The development of these folds is kinematically compatible with a right-lateral component of the movement along the N20° faults (pressure-ridge type).

During Late Miocene the upper layers of the sequence M_2 show a series of progressive unconformities related to syn-sedimentary folding (Figs. 3c & d). This deformation has been observed in all the basins and all the filling (Lavenu & Noblet 1989). Analysis of stratification poles indicates that these are cylindrical folds with N175° or N350° trending subhorizontal axes (Figs. 3c & d). Noblet *et al.* (1988) suggested that the relative dispersal of the fold orientations was due to local re-orientation of stress related to the proximity of the basin boundaries. They have deduced a mean E–W trending shortening.

The interpretation of Noblet *et al.* (1988) and Lavenu & Noblet (1989), based on the analysis of syn-sedimentary fold deformations, proposed that the opening of the Miocene basins in the South Ecuadorian Andes was controlled by N–S and N20°–N40° strike-slip faults. During Early Miocene a transtensional regime occurred and tensional movement perpendicular to the N20°–N40° faults during deposition of sequence M_1 was related to a regional deformation with a NNE–SSW trending shortening. A NE–SW then E–W trending shortening was inferred from analysis of syn-sedimentary folds affecting the Middle to Late Miocene deposits of sequence M_2. It was the origin of respective right-lateral and reverse-right-lateral movements on N20°–N40° and N–S faults, and caused the progressive closing of the basins. The conclusions drawn from these studies stress the fact that the syn-sedimentary deformation occurred throughout the filling of the basins. It suggests the existence of ongoing tectonics with progressive 60° clockwise rotation of the stress component during the Miocene.

MICROTECTONIC ANALYSIS

The purpose of this work is to characterize the stress fields which originated syn-sedimentary Miocene deformation in the intermontane basins of Southern Ecuador. To accomplish this, slip vectors on striated faults were analyzed using the Carey's inversion algorithm (Carey &

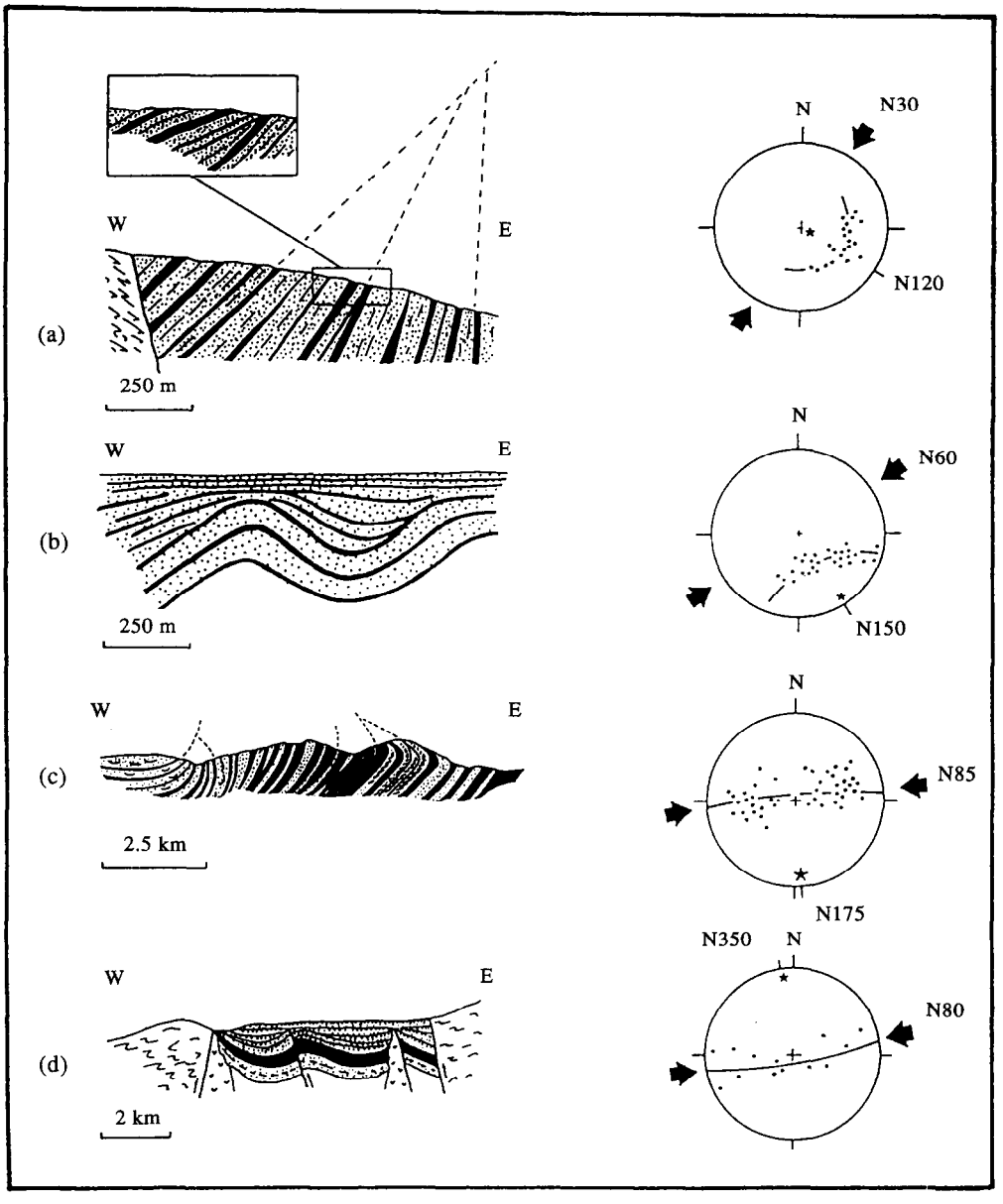

Fig. 3. Cross-sections showing syn-sedimentary deformations and associated fold data. Localizations are on Fig. 1. Points on Wulff stereonets (Lower hemisphere) represent the normal to bedding planes. Stars represent the fold axis. (a) Sedimentary wedges linked to the extensional movements along the NNE–SSW faults. Syn-sedimentary coeval conical folding located along the N20°–N40° faults (Biblian Formation, Cuenca Basin). (b) Syn-sedimentary conical folding located along NNE–SSW faults (N30° compressional direction). (Azogues Formation, Cuenca Basin.) (c) Progressive unconformity provoked by a cylindrical folding (N85° compressional direction). (Mangan Formation, Cuenca Basin.) (d) Folds and progressive unconformity associated with syn-sedimentary faulting (N80° compressional direction). (Quillollaco Formation, Malacatos Basin.)

Brunier 1974, Carey 1979). Fault populations were measured inside or outside the basin limits, in the basement, as well as in sequences M_1 and M_2 of basin infill.

General methodology

The shape and orientation of the stress deviator in the rock can be identified from measurements of striations over a population of faults. Following Bott (1959) who studied the direct problem, several authors (e.g. Carey & Brunier 1974, Armijo & Cisternas 1978, Carey 1979, Etchecopar *et al.* 1981, Armijo *et al.* 1982) explored and treated the inverse problem. This problem can be addressed rather simply, however under the assumption that there is no continuous deformation within the blocks separated by faults and thus no rotation of the fault planes during deformation. All the deformation occurs as relative displacements of rigid blocks along the faults. The direction, sense, and sometimes the amount of sliding on the faults are reflected by striation of the fault surface. If slip on the faults are independent, then the direction of each striation is that of the resolved shear acting on each fault. This condition of independent slip is more nearly reached when slips are small. Four parameters may be determined: the three Euler angles that give the directions of the principal axes of stress, and the parameter $R = (\sigma 2' - \sigma 1')/(\sigma 3' - \sigma 1')$.

The stresses $\sigma 1'$, $\sigma 2'$ and $\sigma 3'$ are the deviatoric of the stress tensor with $\sigma 1' > \sigma 2' > \sigma 3'$. In other words the isotropic component of stress cannot be obtained and the deviatoric component is known only within an arbitrary factor.

In order to characterize a tectonic episode (attitude of the principal axes of stress and the parameter R), a homogeneous population of faults must first be recognized. One homogeneous population of faults means faults kinematically consistent with striations explained by a single stress tensor. Homogeneous populations of faults were identified by a series of tests based on the following steps: (i) faults having similar trends, dips and rakes are grouped together; then, comparison of these different groups is graphically made in order to evaluate their kinematic compatibilities (for instance, left-lateral and right-lateral kinematics observed on faults with similar attitudes are not compatible); (ii) consistent faults are regrouped and a computation of the mean stress tensor is made; then this tensor is applied to the entire population of faults collected on the site; (iii) according to the distribution of the angular deviation (τs) (taken less or equal to 20°) between theoretical striations (τ) derived from the computed mean stress tensor and the actual slickensides (s) used to compute this mean stress tensor, a homogeneous population of faults may be recognized. It must be noted here that two successive different striations on a same fault-plane may be indicative of two successive homogeneous populations of faults and consequently of the relative chronology of tectonic pulses.

Methodology adapted to ongoing deformation

In the South Ecuadorian basins, syn-sedimentary deformations highlight the on-going Neogene tectonics (Noblet *et al.* 1988) displaying a rotation of the shortening direction from NE–SW to WNW–ESE. These well-known larger scale deformations provide a reliable control on microtectonic analysis. They especially allow for sites displaying various populations of faults, as shown by relative chronologies of striations, to be also considered and reliably analysed. A preliminary microtectonic characterization of these deformations using the inverse problem (Winter 1990) suggests that the methodology could be adapted in order to identify successive increments of this on-going Neogene tectonics.

When various homogeneous populations of faults are recognized in the field, a computation of the mean stress tensor is performed on each identified population. The mean stress tensor (Pi) is adjusted in order to characterize a homogeneous population whose angular deviations (τs) between theoretical striations (τ) computed from the mean stress tensor and the actual striations (s) are less or equal to 20°. In this study, the computed stress tensors explained more than 65% of the numerous striations observed. Because these computed stress tensors (Pi) are consistent with the larger-scale syn-sedimentary deformations, they are assumed to be characteristic of major tectonic pulses within an on-going regional tectonic deformation.

In order to be sure that, on each site, no data has been forgotten in the graphical selection of the homogeneous populations which have been used to compute the mean stress tensors, these computed mean tensors are applied to the entire population of faults collected on the site and all striations having an angular deviation lesser or equal to 30° are selected. This value of 30° has been chosen to take into account possible local guided movements. Moreover, it must be noted that the data neglected represent less than 10% of the first selected homogeneous population. In some cases, various striations are explained by two computed stress tensors (Pi and Pj). These common faults are always kinematically consistent and consequently form a homogeneous population ($Pi \cap Pj$) which should be explained by a single stress tensor (p_{i-j}). If there is enough common data (at least eight common data), a mean stress tensor (p_{i-j}) is thus computed from these common striations ($Pi \cap Pj$). Then, it is applied to the entire population of faults collected on the site. In order to constrain this secondary mean stress tensor, only striations with angular deviation (τs) smaller than 20° are selected.

Taking into account the general on-going Neogene tectonics of the region, the secondary mean stress tensor obtained is assumed to be characteristic of an intermediate minor tectonic pulse. However, it must be noted here, that due to the methodology itself, such a minor pulse may reflect either an intermediate brief intensification of the shortening in a given direction during the rotation of the compressive stress or an integration (average) of the whole compressive deformations which occurred between two major tectonic pulses.

For all sites, the computed solutions for major and minor (if any) tectonic pulses are presented in the form of stereonets and histograms of the distribution of the angular deviation between theoretical striations corresponding to the mean stress tensor and the actual striations. When faults common to two major pulses have been evidenced, relative quantities of common and exclusive data are presented on histograms. If a mean stress tensor has been computed from these common striations, relative quantities of (i) data strictly exclusive of each pulse (black areas on Fig. 4), (ii) exclusive data of a major pulses also consistent with the minor intermediate pulse (striped areas on Fig. 4), and (iii) data common to two major pulses and used to compute the mean stress tensor characterizing the intermediate minor pulse (light grey areas on Fig. 4) are presented on these histograms.

The procedure was applied to each measurement site.

Results of the inversion

The sites were investigated from north to south, from Cuenca towards Malacatos, outside the basins or at boundaries as within the basins. Two sites will be analyzed in detail, one simple (Huangarcucho), another

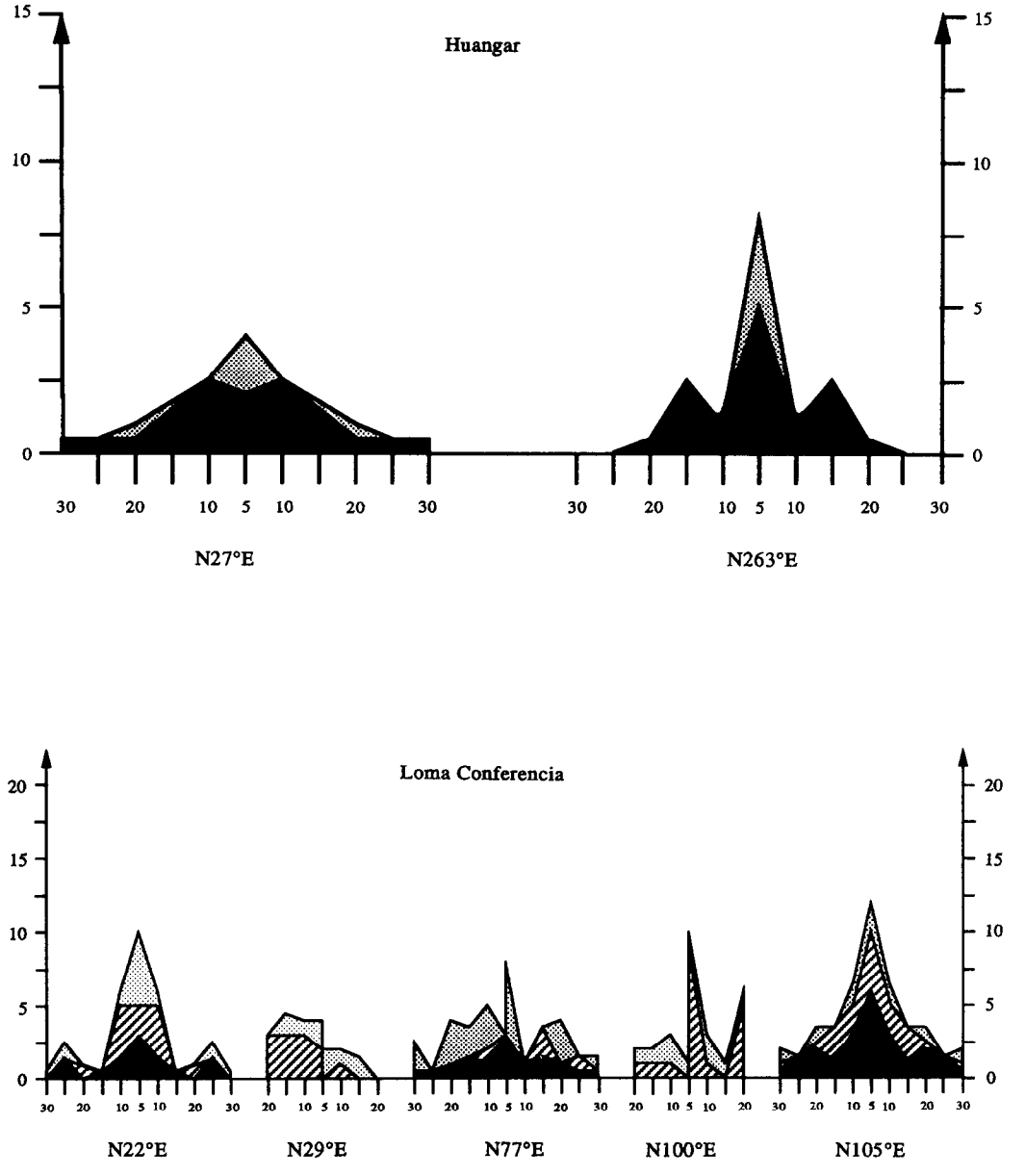

Fig. 4. Major and minor pulses deduced from the analysis of each population of faults. Pulses are identified by the strike of $\sigma 1$. On a pulse histogram, black area represents exclusive faults, light grey area represents faults common to two major pulses (this homogeneous population is used to compute the mean stress tensor of a minor pulse) and striped area represents faults common to one major pulse and one minor pulse.

more complex (Loma Conferencia) (Figs. 4 and 5). All the results are summarized in Fig. 6 and Tables 1–4.

The site of Huangarcucho comprises 29 faults measured in the lower layers of the Cuenca basin sequence M_2, as well as in the rhyolitic basement on the eastern basin boundary. The calculated stress field corresponds to two major pulses. One, $P1$, is characterized by $\sigma 1$: 4°/N27° ($\sigma 2$: 26°/N120° and $\sigma 3$: 63°/N289) with $R = 0.72$. Faults having a N–S direction are reverse with a dextral strike-slip component; faults having a NE–SW direction are reverse with a left-lateral strike-slip component. The other, $P2$, is characterized by $\sigma 1$: 5°/N263° ($\sigma 2$: 37°/N169° and $\sigma 3$: 52°/N362°) with a ratio $R = 0.66$. Faults having a N–S direction are right-lateral strike-slip faults with reverse component; faults having a NE–SW to E–W direction are reverse with a left-lateral strike-slip component. Computations of $P1$ and $P2$ comprise a group of three common faults (light grey area in Fig. 4) representing $P1 \cap P2$. The scarceness of data (<8) does not make it possible to calculate a characteristic minor intermediate pulse.

The Loma Conferencia site, situated within the Cuenca basin in sequence M_1 of Lower Miocene lithostratigaphic unit, is representative of this type of analysis. Analysis of 87 right-lateral and left-lateral faults, after graphical separation into homogeneous populations, makes it possible to determine major and minor tectonic pulses on the site.

During the first step of the work, three significant deviatoric tensors (with $\tau s \leqslant 20°$) can be distinguished. Each of these three tensors helps characterize a major tectonic pulse:

Table 1. Parameters of the stress deviators computed from reverse and strike-slip fault kinematics of lower Miocene ($\sigma 1$: N24°–N48°). *Nd*, number of data used for computation: $\sigma 1$, $\sigma 2$, $\sigma 3$ give the principal stress direction and *R* the stress ratio $(\sigma 2 - \sigma 3)/(\sigma 2 - \sigma 1)$ of the optimum models. *R* varies from 0 for $\sigma 2 = \sigma 1$ to 1 for $\sigma 2 = \sigma 3$

Sites		*Nd*	Lat (S)	Long. (W)	Principal stress directions $\sigma 1$ Az	$\sigma 1$ Dip	$\sigma 2$ Az	$\sigma 2$ Dip	$\sigma 3$ Az	$\sigma 3$ Dip	*R*
Huangarcucho	4HG1	16	2°52′	78°53′	27°	04°	120°	26°	289°	63°	0.72
Rircay	5RI	12	3°17′	79°15′	39°	02°	130°	19°	303°	71°	0.98
Nabón	7CHU1	17	3°18′	79°03′	220°	04°	130°	01°	31°	86°	0.86
	$7CHU_{1-2}$	13	3°18′	79°03′	228°	08°	319°	05°	78°	81°	0.75
Ceibopamba	9CE1	23	4°12′	79°19′	204°	05°	301°	57°	111°	32°	0.27
Loma Conferencia	10LC1	31	3°00′	78°56′	22°	10°	275°	59°	117°	29°	0.89
	$10LC_{1-2}$	20	3°00′	78°56′	29°	04°	121°	24°	290°	66°	0.67
Gordeleg	11GO	17	2°57′	78°54′	43°	13°	134°	06°	247°	76°	0.51
Malacatos	15M1	10	4°13′	79°14′	213°	05°	120°	26°	312°	64°	0.80

Table 2. Parameters of the stress deviators computed from reverse and strike-slip fault kinematics of Middle and Late Miocene ($\sigma 1$: N52°–N64°). *Nd*, number of data used for computation; $\sigma 1$, $\sigma 2$, $\sigma 3$ give the principal stress direction and *R* the stress ratio $(\sigma 2 - \sigma 3)/(\sigma 2 - \sigma 1)$ of the optimum models. *R* varies from 0 for $\sigma 2 = \sigma 1$ to 1 for $\sigma 2 = \sigma 3$

Sites		*Nd*	Lat (S)	Long. (W)	Principal stress directions $\sigma 1$ Az	$\sigma 1$ Dip	$\sigma 2$ Az	$\sigma 2$ Dip	$\sigma 3$ Az	$\sigma 3$ Dip	*R*
Racchahuaicu	IRA1	45	2°51′	78°52′	242°	01°	333°	15°	150°	75°	0.33
Huachun	3HU1	28	3°49′	78°51′	52°	01°	322°	07°	146°	83°	0.92
Sulupali	6SU	19	3°18′	79°16′	57°	14°	222°	76°	326°	03°	0.42
Nabón	7CHU2	23	3°18′	79°03′	245°	14°	145°	01°	52°	76°	0.65
	$7CHU_{2-3}$	11	3°18′	79°03′	243°	06°	333°	05°	99°	82°	0.66
Oña	8ON1	25	3°28′	79°09′	244°	04°	144°	70°	336°	20°	0.67
Ceibopamba	9CE2	14	4°12′	79°19′	243°	26°	36°	61°	147°	11°	0.97
Santa Isabel	13SI	22	3°18′	79°18′	244°	03°	339°	64°	152°	26°	0.84

Table 3. Parameters of the stress deviators computed from reverse and strike-slip fault kinematics of Middle and Late Miocene ($\sigma 1$: N71°–N107°). *Nd*, number of data used for computation; $\sigma 1$, $\sigma 2$, $\sigma 3$ give the principal stress direction and *R* the stress ratio $(\sigma 2 - \sigma 3)/(\sigma 2 - \sigma 1)$ of the optimum models. *R* varies from 0 for $\sigma 2 = \sigma 1$ to 1 for $\sigma 2 = \sigma 3$

Sites		*Nd*	Lat (S)	Long. (W)	Principal stress directions $\sigma 1$ Az	$\sigma 1$ Dip	$\sigma 2$ Az	$\sigma 2$ Dip	$\sigma 3$ Az	$\sigma 3$ Dip	*R*
Racchahuaicu	IRA_{1-2}	34	2°51′	78°52′	81°	08°	351°	03°	243°	82°	0.31
Chocarsi	2CHO1	24	2°52′	78°52′	269°	02°	000°	25°	174°	65°	0.75
	$2CHO_{1-2}$	16	2°52′	78°52′	95°	08°	002°	17°	210°	71°	0.44
Huachun	3HU2	24	3°49′	78°51′	88°	03°	358°	00°	264°	86°	0.98
	$3HU_{1-2}$	21	3°49′	78°51′	252°	03°	343°	25°	157°	65°	0.82
Huangarcucho	4HG2	16	2°52′	78°53′	263°	05°	169°	37°	362°	52°	0.66
Nabón	7CHU3	18	3°18′	79°03′	277°	08°	8°	03°	119°	81°	0.62
Oña	8ON2	23	3°28′	70°09′	81°	04°	172°	11°	332°	78°	0.80
	$8ON_{1-2}$	22	3°28′	79°09′	260°	02°	167°	56°	351°	34°	0.86
Ceibopamba	9CE3	44	4°12′	79°19′	94°	15°	345°	51°	195°	36°	0.74
Loma Conferencia	10LC2	30	3°00′	78°56′	77°	10°	172°	27°	328°	60°	0.43
	10LC3	44	3°00′	78°56′	105°	08°	12°	19°	218°	69°	0.94
	$10LC_{2-3}$	25	3°00′	78°56′	100°	11°	194°	20°	343°	67°	0.79
Molobog	12MO	22	2°37′	78°52′	279°	04°	11°	23°	180°	67°	0.60
Loja	14BO	26	3°57′	79°13′	101°	09°	192°	06°	316°	80°	0.65
Malacatos	15M2	16	4°13′	79°14′	287°	03°	18°	19°	189°	71°	0.93
Masanamarca	16M	12	4°19′	79°13′	251°	07°	160°	02°	52°	82°	0.93

— *P*1 with $\sigma 1$: 10°/N22°, $\sigma 2$: 59°/N275°, $\sigma 3$: 29°/N117° and $R = 0.89$;
— *P*2 with $\sigma 1$: 10°/N77°, $\sigma 2$: 27°/N172°, $\sigma 3$: 60°/N328° and $R = 0.43$;
— *P*3 with $\sigma 1$: 8°/N105°, $\sigma 2$: 19°/N12° $\sigma 3$: 69°/N218° and $R = 0.94$.

The test of each deviatoric tensor applied to all of the striations measured on the site make it possible to determine new fault populations for which $\tau s \leqslant 30°$. This, for *P*1 ($\sigma 1$: 10°/N22°), 30 compatible faults, for which 20 are exclusive to the tensor can be identified (black area on Fig. 4), for *P*2 ($\sigma 1$: 10°/N77°) 30 compat-

Table 4. Parameters of the stress deviators computed from reverse and strike-slip fault kinematics of Middle and Late Miocene ($\sigma1$: N114°–N130°). *Nd*, number of data used for computation; $\sigma1$, $\sigma2$, $\sigma3$ give the principal stress direction and *R* the stress ratio $(\sigma2 - \sigma3)/(\sigma2 - \sigma1)$ of the optimum models. *R* varies from 0 for $\sigma2 = \sigma1$ to 1 for $\sigma2 = \sigma3$

Sites		*Nd*	Lat (S)	Long. (W)	Principal stress directions						
					$\sigma1$		$\sigma2$		$\sigma3$		
					Az	Dip	Az	Dip	Az	Dip	*R*
Racchahuaicu	1RA2	49	2°51′	78°52′	114°	20°	019°	13°	259°	66°	0.48
Chocarsi	2CHO2	22	2°52′	78°52′	129°	05°	038°	13°	238°	76°	0.47
Huachun	3HU3	20	3°49′	78°51′	130°	30°	33°	12°	284°	57°	0.37
Oña	8ON3	19	3°28′	79°09′	305°	09°	214°	06°	90°	79°	0.25

ible faults, of which 20 are exclusive to the tensor can be identified (black area on Fig. 4), and for *P*3 ($\sigma1$: 8°/N105°) 44 compatible faults, 36 of which are exclusive to the tensor, can be identified (black area on Fig. 4).

In the second step, analysis helps determine minor tectonic pulses. Computations of *P*1 and *P*2 comprise a group of 10 common faults (light grey on the histogram), representing $P1 \cap P2$. Calculations of *P*2 and *P*3 include a set of eight common faults ($P2 \cap P3$). These intersections, p_{1-2} and p_{2-3} include at least eight striations. They make it possible to calculate characteristic tensors p_{1-2} and p_{2-3} which correspond to minor tectonic pulses on the site:

— p_{1-2} corresponds to $\sigma1$: 4°/N29°, $\sigma2$: 24°/N121°, $\sigma3$: 66°/N290° and $R = 0.67$;
— p_{2-3} corresponds to $\sigma1$: 11°/N100°, $\sigma2$: 20°/N194°, $\sigma3$: 67°/N343° and $R = 0.79$.

Tests of the new tensors on all the faults of the site make it possible to select two groups of striated faults with $\tau s \leqslant 20°$. Thus, for p_{1-2} ($\sigma1$: 4°/N29°), 21 compatible faults can be identified. None of them are exclusive: 11 are common with *P*1, ($P1 \cap p_{1-2}$: striped area on histogram (Fig. 4)), one is common with *P*2, ($P2 \cap p_{1-2}$: striped area on histogram (Fig. 4)) and nine are common with *P*1 and *P*2 ($P1 \cap P2$: light area on histogram (Fig. 4)). For p_{2-3} ($\sigma1$: 11°/N100°) 25 compatible faults can be identified. None of them are exclusive; 14 are common with *P*3, ($P3 \cap p_{2-3}$: striped area on histogram (Fig. 4)), three are common with *P*2 ($P2 \cap p_{2-3}$: striped area on histogram (Fig. 4)) and nine are common with *P*2 and *P*3 ($P2 \cap P3$: light grey area on histogram (Fig. 4)). Striations with angular deviations $\tau s > 20°$ are not retained for the calculation.

The determination of minor pulses p_{1-2} and p_{2-3} reveals that the major pulse *P*2 can be decomposed into several sets: 10 exclusive faults (black area in Fig. 4), one common fault ($P1 \cap p_{1-2}$: left striped area on Fig. 4), 10 common faults ($P1 \cap P2$: left light grey area on Fig. 4), eight common faults ($P2 \cap P3$: right light grey area on Fig. 4), three common faults ($P2 \cap p_{2-3}$: left striped area on Fig. 4).

The pulses *P*1 (N22°) and p_{1-2} (N29°) are very similar in trend, but the first one is the consequence of a strike-slip regime ($\sigma3$ horizontal) while the second is the consequence of a compressive regime ($\sigma3$ vertical). Such a change should be related to an increase of the horizontal stresses.

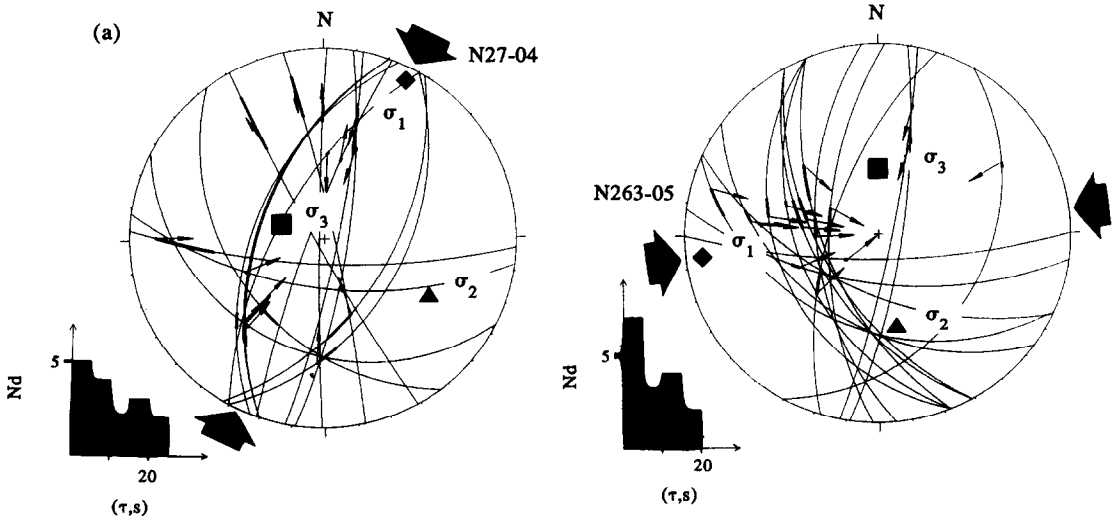

Fig. 5. Slip vector data from Neogene reverse and strike-slip faults of Southern Ecuadorian continental basins. Arrow attached to fault traces corresponds to the measured slip vectors (Wulff stereonet, lower hemisphere). Thick segments on the fault traces and histograms show deviations between measured (s) and predicted (τ) slip vectors on each fault plane. Convergent large black arrows give azimuths of the computed maximum principal stress $\sigma1$ direction. (a) Huangarcucho site, (b) Loma Conferencia site. Histograms (*Nd*, τs) represent the distribution of the angular deviation between measured (s) and predicted (τ) slip vectors.

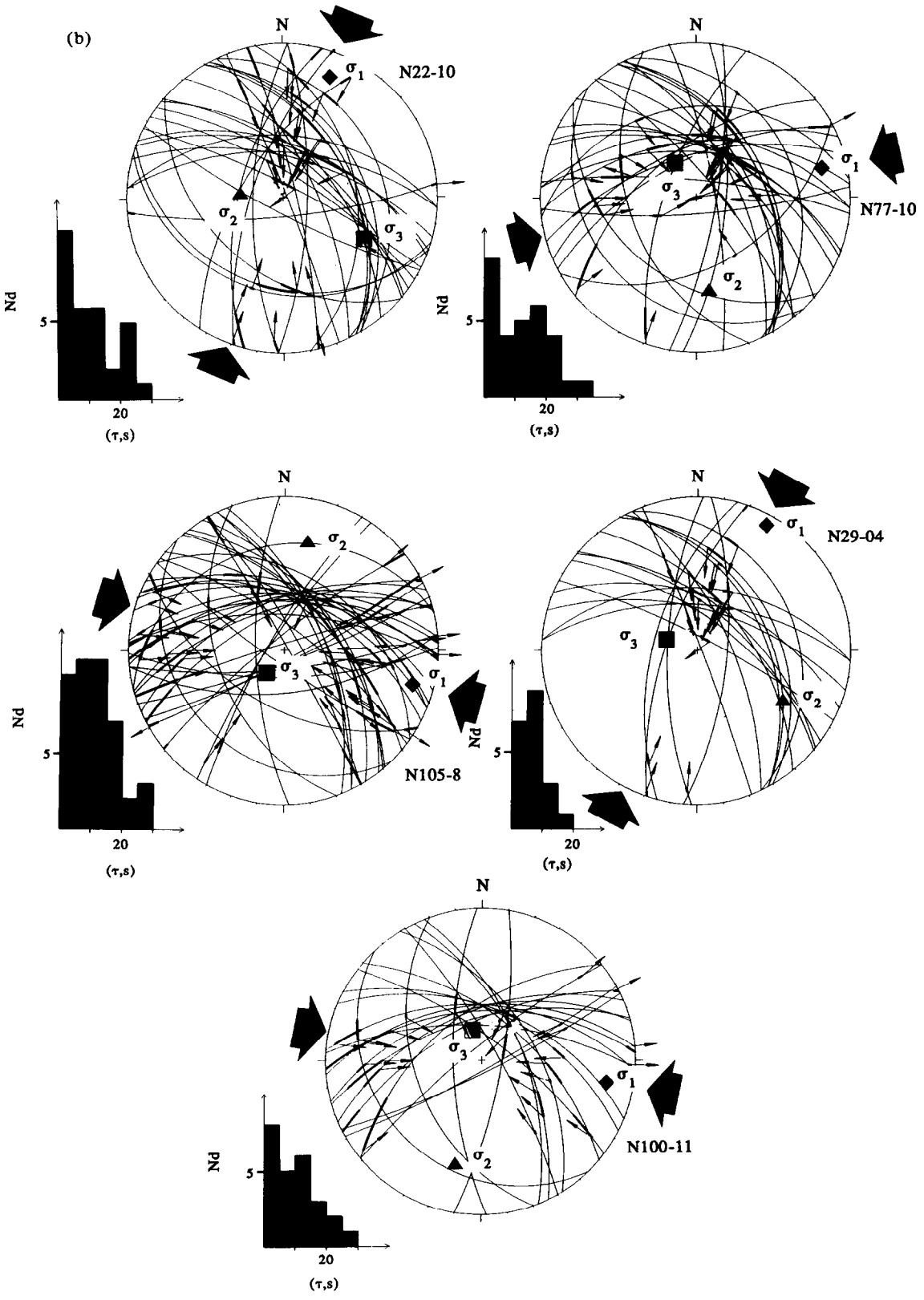

Fig. 5. Continued.

Interpretation

This microtectonic study of the infill and the basement of the South Ecuadorian Andean basins allows us to characterize each principal stage of the ongoing compressive stress regime during at least the Miocene period. In sediments of sequence M_2 (Middle and Late Miocene), the direction of the major stress component, $\sigma 1$, is between N71° and N107° (Molobog, Loja, Malacatos, Masanamarca; Table 3). The microtectonic analysis of sites measured in the sequence M_1 and in the basement also display $\sigma 1$ orientations varying from N71° to

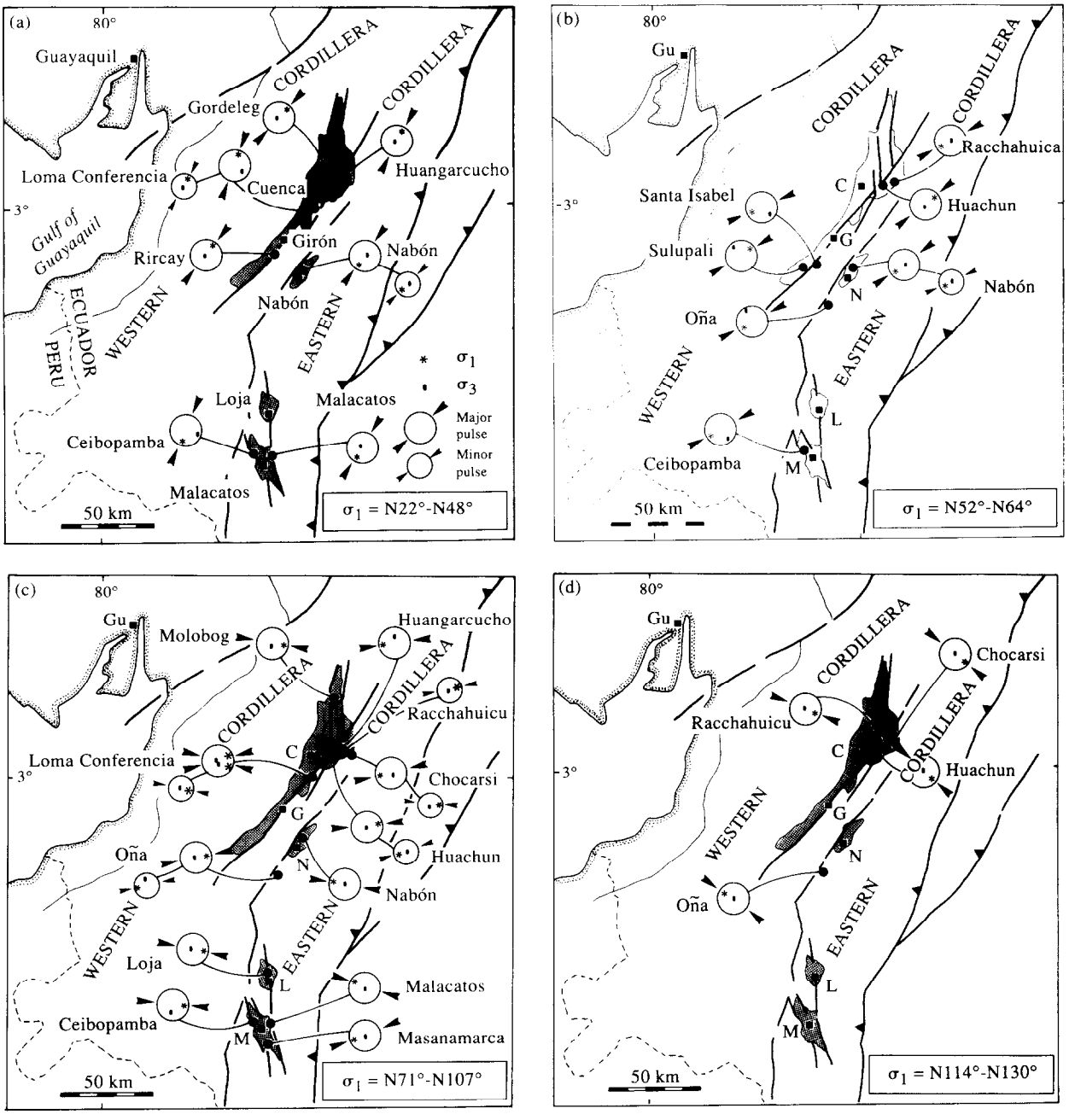

Fig. 6. Principal compressional stress directions deduced from kinematics of reverse and strike-slip faults of Lower Miocene to Upper Miocene. (a) $\sigma 1$: N24°–N48°, (b) $\sigma 1$: N52°–N64°, (c) $\sigma 1$: N71°–N107°, (d) $\sigma 1$: N114°–N130°.

N107° (Racchahuiacu, Chocarsi, Huachun, Huangarcucho, Nabón, Oña, Ceibopamba). If this compression is removed from results obtained in sites measured in the basement and in sequence M_1 of the basin, the main $\sigma 1$ directions remaining are N22°–N48° (Table 1) and N52°–N64° (Table 2). This implies that, at least during the Early Miocene, the South Ecuadorian basins were subject to a NNE–SSW to NE–SW trending compression. Slickensides in the Racchahuiacu site show a relative chronology of the striations which is coherent with this chronology: a NE–SW compression followed by an E–W compression, as deduced from a comparison of inversion results for all the measured sites.

Only four sites measured in the basement or along main faults (Table 4) show an ENE–WSW trending compression. On sites Racchahuiacu and Huangarcucho, analysis of the chronology between the striations shows that this compression is the younger.

In each two major groups of compression, NE–SW and E–W, some sites have permitted several solutions (tensor) to be computed. The relative chronologies of striations suggest that these tensors occurred one after the other. For example, in site Loma Conferencia the major event $\sigma 1$: N22° occurred before event $\sigma 1$: N29°, likewise, events $\sigma 1$: N77°, $\sigma 1$: N100° and $\sigma 1$: N105° chronologically follow one another. This indicates a rotation of the stress.

Thus, the microtectonic analysis helps determine a series of successive tectonic pulses during the Miocene. Initially, no continuation is discerned from one pulse to

another. This is due to the methodology. The ongoing tectonics is demonstrated only by the syn-sedimentary deformations whereas the microtectonic analysis leads to computation of stress tensors which characterize certain increments of the deformation.

DISCUSSION AND CONCLUSION

Microtectonic analysis has revealed a compressive state of stress with $\sigma 1$ in a NNE–SSW direction in the Early Miocene. The normal component of movement, observed on faults striking N20°–N40°, is compatible with this Early Miocene stress field, if $\sigma 2$ is vertical and if the N–S faults were formed earlier. The stress field, identified from sites Huangar, Rircay, Nabón, and Loma Conferencia, is characterized by very close main stress components $\sigma 3$ and $\sigma 2$ ($R \approx 1$). Consequently their axes may become permuted depending on local parameters (e.g. proximity of a major fault). The variation in deviations between tectonic pulses might also be caused by local deviations produced by major faults. Results of the microtectonic analysis, the sedimentological study and the analysis of syn-sedimentary deformations, suggest that the Early Miocene deepening, marked by fining-upward and thinning-upward in the sedimentation (M_1), is the consequence of right-lateral strike-slip movements along N–S faults and right-lateral-normal movements along N20°–N40° faults. The state of stress is characterized by $\sigma 1$ and $\sigma 3$ horizontal (Sulupali, Oña, Ceibopamba, Loma Conferencia, Santa Isabel).

The stress field in the Middle and Late Miocene is characterized by a subhorizontal $\sigma 1$ striking approximately E–W. Almost half of the results obtained (43%) displays a $\sigma 1$ direction between N71° and N107°. The relative magnitudes of $\sigma 3$ and $\sigma 2$ are generally quite similar (for 83%, $R > 0.5$, and for 50%, $R > 0.70$). Study of syn-sedimentary folds has indicated shortening directions varying between N60° at the base of M_2, to N80°–N130° at the top of M_2 (Lavenu & Noblet 1988). M_2 shows coherence between results of fold analysis and microtectonic analysis. Results of microtectonic, sedimentological and syn-sedimentary fold analyses, suggest that the basin infilling, marked in the Middle and Late Miocene by coarsening-upward and thickening-upward in M_2, is probably due to movements with a strong reverse component along N–S and N20° faults.

In Southern Ecuador, the suggested ongoing compressive tectonics interpretation of Noblet *et al.* (1988) counters the currently accepted notion of short tectonic phases (1–2 Ma) in the Central Andes (Dalmayrac *et al.* 1980, Mégard 1978, Sébrier *et al.* 1988). Four compressive phases have been described in the Central Andes (review in Sébrier *et al.* 1988 and Sébrier & Soler 1991), covering a period from the late Oligocene to the Pliocene (Quechua Period): F_2, late Oligocene (28–26 Ma) with $\sigma 1$: NNE–SSW: F_3, Early Miocene (17–15 Ma) with $\sigma 1$: N–S in Central Peru and $\sigma 1$: E–W in the South Peruvian Pacific Piedmont; F_4, Middle Miocene (10 Ma) with $\sigma 1$: N–S in Central Peru and $\sigma 1$: E–W in the South Peruvian Pacific Piedmont; finally, F_5, Late Miocene (7 Ma) with $\sigma 1$: E–W.

The chronology of these compressive phases is generally established from dating on regional unconformities. In Ecuador, such a determination of tectonic phases from regional unconformities would have led to an initial significant tectonic phase in Southern Ecuador, during the Late Oligocene (between 26 and 24.7 Ma), a local tectonic phase in the early Miocene (between 20 and 16 Ma) and a last tectonic phase in the Late Miocene (between 8 and 7.1 Ma).

However, in Southern Ecuador, excepting the direction of the shortening in the Middle Miocene, Miocene shortening directions in the South Ecuadorian basins are consistent with those determined in Central Peru. As in the Central Andes (Pardo-Casas & Molnar 1987), there is a good correlation between the rapid Neogene convergence and the period during which the south Ecuadorian continental basins were deformed by compression (Quechua Period).

In Southern Ecuador, combined studies of stratigraphy, sedimentology, syn-sedimentary deformations and microtectonics show that a continuous deformation probably affected all the basins during the whole Miocene. The same kind of approach performed in the Neogene sedimentary basins of Central Andes might determine if the geodynamics of Southern Ecuador is only an exception, or a general pattern at the scale of the Andes.

Acknowledgements—This work formed part of research supported by the Institut Français de Recherche Scientifique pour le Développement en Coopération (ORSTOM) [IPGH-EPN-CLIRSEN-ORSTOM Convention in Ecuador] and Institut Français d'Etudes Andines (IFEA). Mark Cooper and Alessandro Tibaldi are greatly acknowledged for constructive and thorough reviews. We thank René Marocco for fruitful discussions and Anne-Marie Wawrzkow for her helpful English translation. Unité de Recherche "Géodynamique et Concentrations Minérales" ORSTOM Contribution.

REFERENCES

Angelier, J. & Goguel, J. 1979. Sur une méthode simple détermination des axes principaux des contraintes pour une population de failles. *C.r. Acad. Sci. Paris* **D288**, 307–310.

Armijo, R., Carey, E. & Cisternas, A. 1982. The inverse problem in microtectonics and the separation of tectonic phases. *Tectonophysics* **82**, 145–160.

Armijo, R. & Cisternas, A. 1978. Un problème inverse en microtectonique cassante. *C.r. Acad. Sci. Paris* **D287**, 595–598.

Baldock, J. W. 1982. Geology of Ecuador: explanatory Bulletin of the National Geological Map of the Republic of Ecuador. Esc. 1:1,000,000, Min. Rec. Nat. Energ., Quito.

Barberi, F., Cotelli, M., Ferrara, G., Innocenti, F., Navarro, J. M. & Santacroce, R. 1988. Plio-Quaternary volcanism in Ecuador. *Geol. Mag.* **125**, 1–14.

Blair, T. C. & Bilodeau, W. L. 1988. Development of tectonic cyclotherms in rift, pull apart and foreland basins: sedimentary response to episodic tectonism. *Geology* **16**, 517–520.

Bott, M. H. P. 1959. The mechanics of oblique slip faulting. *Geol. Mag.* **XCVI**, 109–117.

Bristow, C. R. 1973. Guide to the geology of the Cuenca Basin, southern Ecuador. Ecuadorian Geol. Geophys. Soc.

Bristow, C. R. & Parodiz, J. J. 1982. The stratigraphical paleontology of the Tertiary non-marine sediments of Ecuador. *Bull. Carn. Mus. Nat. Hist.* **19**.

Burke, K. 1988. Tectonic evolution of the Caribbean. *Annu. Rev. Earth & Planet. Sci.* **16**, 201–230.

Butler, K. 1974. Ecuadorian Andes. In: *Mesozoic–Cenozoic Orogenic Belts: Data for Orogenic Studies* (edited by Spencer, A. M.). Scottish Academic Press, Edinburgh, 725–740.

Carey, E. 1979. Recherche des directions principales de contraintes associées au jeu d'une population de failles. *Rev. Géogr. Phys. Géol. Dyn.* **21**, 57–66.

Carey, E. & Brunier, B. 1974. Analyse théorique et numérique d'un modèle élémentaire appliqué à l'étude d'une population de failles. *C.r. Acad. Sci. Paris* **D269**, 891–894.

Case, J. E. 1974. Major basins along continental margin of Northern South America. In: *The Geology of Continental Margins* (edited by Burk, C. A. & Drake, C. L.). Springer-Verlag, New York, 733–742.

Case, J. E., Shagam, R. & Giegengack, R. F. 1990. Geology of the Northern Andes: an overview. In: *The Caribbean Region* (edited by Dengo, G. & Case, J. E.). The Geology of North America, *Geol. Soc. Am.* Vol. H, 177–200.

Dalmayrac, B., Laubacher, G. & Marocco, R. 1980. Caractères généraux de l'évolution géologique des Andes péruviennes. Travaux et Documents ORSTOM, 122, Paris.

Daly, M. C. 1989. Correlations between Nazca/Farallon plate kinematics and forearc basin evolution in Ecuador. *Tectonics* **8**, 769–790.

Direccion General de Geologia y Minas (DGGM) 1974. Mapa geológico del Ecuador, 1/50,000, hoja Azogues, Ministerio de Recursos Naturales y Energeticos, Quito.

Direccion General de Geologia y Minas (DGGM) 1982. Mapa geológico del Ecuador, 1/1,000,000. Ministerio de Recursos Naturales y Energeticos, Quito.

Egüez, A. & Noblet, Ch. 1988. Nuevos datos estratigraficos de la cuenca de Cuenca (Sur del Ecuador): implicaciones geologicas y geodinamicas. *Pol. Mono. de geologia.* **XIII**, 33–47.

Etchecopar, A., Vasseur, G. & Daignières, M. 1981. An inverse problem in microtectonics for the determination of stress tensors from fault striation analysis. *J. Struct. Geol.* **3**, 51–65.

Fierro, J. 1991. Estudio geodinámico de la cuenca intramontãnosa cenozoica de Malacatos (Sur del Ecuador). Unpublished thesis, E.P.N., Quito, Ecuador.

Izquierdo, O. 1991. Estudio geodinámico de la cuenca intramontãnosa cenozoica de Loja (Sur del Ecuador). Unpublished thesis, E.P.N., Quito, Ecuador.

Jordan, T. E., Isacks, B. L., Allmendinger, J. A., Brewer, J. A., Ramos, V. A. & Ando, C. J. 1983. Andean tectonics related to geometry of subducted Nazca plate. *Bull. geol. Soc. Am.* **94**, 341–361.

Kennerley, J. B. 1980. Outline of the geology of Ecuador. *Overseas Geol. & Miner. Resour.* **55**.

Lavenu, A. & Noblet, C. 1989. Syn-sedimentary tectonic control of Andean intermontane strike-slip basins of South Ecuador (South America). Int. Symp. on Intermontane Basins: Geology and Resources: 306–317, Chiang Mai, Thailand.

Lavenu, A., Noblet, C., Bonhomme, M. G., Egüez, A., Dugas, F. & Vivier, G. 1992. New K/Ar age dates of Neogene and Quaternary volcanic rocks from the Ecuadorian Andes: implications for the relationships between sedimentation, volcanism, and tectonics. *J. S. Am. Earth Sci.* **5**, 309–320.

Lebrat, M. 1985. Caractérisation géochimique du volcanisme anté-orogénique de l'Occident équatorien: implications géodynamiques. Doc. et Trav. CGGM, 6, Montpellier, France.

Lebrat, M., Mégard, F. & Dupuy, Cl. 1985a. Pre-orogenic volcanic assemblages and position of the suture between oceanic terranes and the South American continent in Ecuador. *Zentbl. Miner. Geol. Paläont.* **H9–10**, 1207–1214.

Lebrat, M., Mégard, F., Juteau, T. & Calle, J. 1985b. Pre-orogenic volcanic assemblages and structure in the western Cordillera of Ecuador between 1°40′S and 2°20′S. *Geol. Rdsch.* **74**, 685–713.

Madden, R. H. 1990. Miocene Toxodontidae (Notoungulata, Mammalia) from Colombia, Ecuador and Chile. Ph.D. thesis, Duke University.

Marshall, W. B. & Bowles, E. O. 1932. New fossil fresh water mollusks from Ecuador. *Proc. U.S. Natl. Mus.* **82**, 2946: 1–7.

Mediavilla, J. 1991. Evolución geodinámica de la cuenca terciaria de Girón-Santa Isabel, Sur del Ecuador. Unpublished thesis, E.P.N., Quito, Ecuador.

Mégard, F. 1978. Etude Géologique des Andes du Pérou central. Mémoire ORSTOM, 86, Paris.

Mégard, F. 1987. Cordilleran Andes and marginal Andes: a review of andean geology north of the Arica elbow (18°S). In: *Circum-Pacific Orogenic Belts and Evolution of the Pacific Ocean Basin* (edited by Monger, J. H. & Francheleau, J.). *Am. Geophys. Un. Geodyn. Ser.* **18**, 71–95.

Moody, J. D. & Hill, M. J. 1956. Wrench-fault tectonics. *Bull geol. Soc. Am.* **67**, 1207–1246.

Noblet, C., Lavenu, A. & Schneider, F. 1988. Etude géodynamique d'un bassin intramontagneux tertiaire sur décrochements dans les Andes du sud de l'Equateur: l'example du bassin de Cuenca. *Géodynam.* **3**, 117–138.

Noblet, C. & Marocco, R. 1989. Lacustrine megaturbidites in an intermontane strike-slip basin: the Miocene Cuenca Basin of South Ecuador. International Symposium on Intermontane Basins: Geology and Resources: 282–293, Chiang Mai, Thailand.

Pardo-Casas, F. & Molnar, P. 1987. Relative motion of the Nazca (Farallon) and South America plates since Late Cretaceous time. *Tectonics* **6**, 233–248.

Robalino, S. 1988. Sedimentacion continental sin-tectonica de la cuenca miocenica de Cuenca. Tesis de Ingenieria, Escuela Politecnica Nacional, Quito.

Sébrier, M., Lavenu, A., Fornari, M. & Soulas, J. P. 1988. Tectonics and uplift in Central Andes (Peru, Bolivia and northern Chile) from Eocene to Present. *Géodynam.* **3**, 85–106.

Sébrier, M. & Soler, P. 1991. Tectonics and magmatism in the Peruvian Andes from Late Oligocene to Present. In: *Andean Magmatism and its Tectonic Setting. Spec. Pap. geol. Soc. Am.* **265**, 259–278.

Winkler, W., Egüez, A., Seward, D., Ford, M. Heller, F., Hungerbühler, D. & Steinmann, M. 1993. A short-lived compression related sediment fill in the Andean intermontane Basin of Nabón (Late Miocene) southern Ecuador. II° ISAG, 321–324, Oxford.

Winter, Th. 1990. Mécanismes des déformations récentes dans les Andes Equatoriennes. Thése de Doctorat, Univ. de Paris-Sud, Orsay.

Zolnai, G. 1989. Continental wrench-tectonics and hydrocarbon habitat. A.A.P.G., Continuing Education Course Notes.